Analysis of Milling Stability by the Chebyshev Collocation Method: Algorithm and Optimal Stable Immersion Levels

Eric A. Butcher and Oleg A. Bobrenkov
Department of Mechanical and Aerospace Engineering
New Mexico State University
Las Cruces NM 88001

Ed Bueler
Department of Mathematics and Statistics
University of Alaska Fairbanks
Fairbanks AK 99775

Praveen Nindujarla
Department of Mechanical Engineering
University of Alaska Fairbanks
Fairbanks AK 99775

Abstract

In this paper the dynamic stability of the milling process is investigated through a single degree-of-freedom model by determining the regions where chatter (unstable) vibrations occur in the two-parameter space of spindle speed and depth of cut. Dynamic systems like milling are modeled by delay-differential equations (DDEs) with time-periodic coefficients. A new approximation technique for studying the stability properties of such systems is presented. The approach is based on the properties of Chebyshev polynomials and a collocation expansion of the solution. The collocation points are the extreme points of a Chebyshev polynomial of high degree. Specific cutting force profiles and stability charts are presented for the up- and down-milling cases of one or two cutting teeth and various immersion levels with linear and nonlinear regenerative cutting forces. The unstable regions due to both secondary Hopf and flip (period-doubling) bifurcations

are found, and an in-depth investigation of the optimal stable immersion levels for down-milling in the vicinity of where the average cutting force changes sign is presented.

1. Introduction

One of the main obstacles to further advancement of milling is the challenge of eliminating the regenerative vibrations commonly referred to as *chatter*. Such vibrations, which adversely affect tool life, process economics, and surface integrity of the machined product, are due to the regenerative mechanism of cutting the surface formed in the previous cut. A stability chart is commonly used to indicate stable (chatter-free) cutting as a function of the spindle speed and depth of cut. It has long been recognized that substantial gains in productivity can be achieved by exploiting the lobed nature of the stability chart, particularly at high speeds [1-3]. This has enabled manufacturers to avoid chatter and to implement high speed machining with much success [4]. For machining processes such as milling the regenerative effect appears in the mathematical model in the form of a *time-delay*, where the delay period is the time between successive cuts of adjacent cutting flutes. Unlike the turning process in which the cutting tool remains stationary, the cutting tool in milling rotates with respect to the workpiece and produces time-periodic coefficients as well as time-delay in the mathematical model, which is a time-periodic *delay differential equation* (DDE) [5]. While analytical methods exist to find the stability boundaries for DDEs with constant coefficients, in general the stability criteria of periodic DDE systems cannot be given in a closed form, and an approximation method is needed.

Minis and Yanushevsky [6] used Fourier series expansions for periodic terms and determined the Fourier coefficients of related parametric transfer functions. Altintas and Budak [7] used a similar method except that they retained only the constant term in each Fourier series expansion of a periodic term. Davies *et al.* [8] and Zhao and Balachandran [9] examined how the periodic motions lost stability during partial immersion milling operations. Davies *et al.* [10] presented experimental results for milling operations with long, slender endmills, which indicate that the consideration of regenerative effects alone may not be sufficient to explain loss of stability of periodic motions for certain partial immersion operations. Davies *et al.* [11] showed the existence of period-doubling instability lobes along with the traditional Hopf instability lobes in low-immersion milling where the cutting time is negligible. The same results were later shown for finite cutting times by Insperger and Stépán [12,13] using the semi-discretization method [14] and by Mann *et al.* [15-17] using the method of temporal finite elements [18]. These methods which lead to stability analysis of discrete maps, are not restricted to infinitesimal times in the cut. Insperger *et al.* [19] and Mann *et al.* [20] analyzed the stability conditions for up- and down-milling operations using the semi-discretization method. The authors restricted their study to a single degree-of-freedom milling model with a linear cutting force and a single cutting tooth. Subsequently, they found the chatter frequencies for secondary Hopf bifurcations and period doubling bifurcations at the stability boundaries [21]. Isolated islands of instability due to the periodicity of the process [22] or nonzero helix angles [23,24] have recently been discovered. Most

recently, the milling process has been investigated for the special cases of variable time-delays [25], variable pitch [26], and state-dependent regenerative delay [27].

The present work presents a new efficient approximation technique for stability analysis of the partial immersion milling process. The method uses a collocation expansion of the solution at the Chebyshev collocation points during the cutting period, and a state transition matrix for the free-vibration period where no cutting occurs. This method is an extension of the Chebyshev-based numerical methods developed by Sinha and Wu [28] for the stability analysis of time-periodic ODEs and by Butcher *et al.* [29] for the stability analysis of time-periodic DDEs with smooth coefficients by Chebyshev polynomial expansion. However, the collocation method proposed here is more efficient than the earlier method of polynomial expansion. Unlike that method, it can easily be applied to periodic DDEs with non-smooth coefficients, in which a portion of the period corresponds to an autonomous ODE.

Collocation methods appear in the literature for solving DDE initial value problems [30, 31] and for finding periodic solutions of nonlinear DDEs [32]. The use of such methods for addressing DDE stability problems is explored in [33, 34]. The method of this paper has several advantages for stability problems, however. First of all, an explicit method for approximating the compact monodromy operator [35] is proposed. Secondly, the action of the spectral differentiation matrix, and thus of the approximate monodromy operator, can be computed by a modification of the Fast Fourier Transform [36]. Next, the exact solution during the period in which the coefficients of the time-delay vanish is utilized in a similar way to [15-17]. Finally, computable uniform error bounds

on the error in the solution and also the error in the approximate Floquet multipliers have been found [37], and a sketch of an *a priori* proof of convergence for the method has been given [38]. The proposed method easily extends to systems with many degrees of freedom, and it produces stability charts with high speed and accuracy for a given parameter range. Other than a preliminary version of this work in [39], this algorithm has also been recently used for dimensional reduction of nonlinear periodic DDEs [40], and for parameter estimation in nonlinear time-varying ODEs [41].

In this paper, specific cutting force profiles and stability charts are produced for the cases of up-milling and down-milling with one or two cutting teeth and various immersion levels with linear and nonlinear regenerative cutting forces. The unstable regions due to both secondary Hopf and flip bifurcations are found, and an in-depth investigation of the optimal stable immersion level for down-milling (where the average cutting force changes from negative to positive) and its implication for increased cutting efficiency in the milling process is presented. The resulting differences between assuming linear versus nonlinear regenerative cutting forces are highlighted.

2. Chebyshev Collocation Method

The Chebyshev collocation method is based on the properties of the Chebyshev polynomials. The standard formula to obtain the Chebyshev polynomial of degree *j*, which is denoted by $T_j(t)$ is

$$T_j(t) = \cos j\theta\,,\ \theta = \arccos(t)\,,\ -1 \le t \le 1 \tag{1}$$

The *Chebyshev collocation points* are unevenly spaced points in the domain [-1,1] corresponding to the extreme points of the Chebyshev polynomial of degree $N \geq 1$. As seen in Fig. 1a), these points are the projections of $N+1$ equispaced points on the upper half of the unit circle:

$$t_j = \cos(j\pi / N), \qquad j = 0, 1, \ldots\ldots, N \tag{2}$$

A spectral differentiation matrix for the Chebyshev collocation points is obtained by interpolating a polynomial through the collocation points, differentiating that polynomial, and then evaluating the resulting polynomial at the collocation points [36]. We can describe the entries of the differentiation matrix D for any order *N* as follows: For each $N \geq 1$, let the rows and columns of the $(N+1)\times(N+1)$ Chebyshev spectral differentiation matrix D be indexed from 0 to *N*. The entries of this matrix are

$$D_{00} = \frac{2N^2+1}{6}, \qquad D_{NN} = -\frac{2N^2+1}{6},$$

$$D_{jj} = \frac{-t_j}{2(1-t_j^2)}, \qquad j = 1, \ldots\ldots, N\text{-}1 \tag{3}$$

$$D_{ij} = \frac{c_i}{c_j}\frac{(-1)^{i+j}}{(t_i - t_j)}, \qquad i \neq j,\ i, j = 0, \ldots\ldots, N$$

$$c_i = \begin{cases} 2, & i = 0, N \\ 1, & otherwise \end{cases}$$

The dimension of D is $(N+1)\times(N+1)$. Since we will need a spectral differentiation matrix for systems of n equations, let the $(N+1)n\times(N+1)n$ differentiation matrix $\mathbb{D}$ be defined as

$$\mathbb{D} = D \otimes I_n \tag{4}$$

where I_n is the $n \times n$ identity matrix and $\otimes$ represents the Kronecker product.

Now consider a system of *n* linear, time periodic DDEs with fixed delay $\tau > 0$,

$$\begin{aligned} \dot{x}(t) &= A(t)x(t) + B(t)x(t-\tau) \\ x(t) &= \phi(t), \quad -\tau \le t \le 0 \end{aligned} \tag{5}$$

where $x(t)$ is a $n \times 1$ state vector, $A(t) = A(t+T)$ and $B(t) = B(t+T)$ are $n \times n$ periodic matrices, and $\phi(t)$ is an $n \times 1$ initial vector function in the interval $[-\tau, 0]$. Here, we only consider the case where $\tau = T$ (which holds for the milling model). However, the version of the Chebyshev collocation code in [42] also extends to the case of multiple discrete delays which are rationally related to each other and to the period *T*.

Unfortunately, because the system matrices in Eq. (5) vary with time, it is not possible to obtain an exponential-polynomial characteristic equation as in an autonomous DDE. As in a periodic ODE, however, a dynamic map may be defined as

$$m_x(i) = U m_x(i-1). \tag{6}$$

that maps the initial vector function $\phi(t)$ in the interval $[-\tau, 0]$ to the state of the system in the first period $[0, \tau]$, and subsequently to each period thereafter. Here m_x represents an expansion of the solution *x(t)* in some basis during either the current or previous period and $m_x(0) = m_\phi$ represents the expansion of $\phi(t)$. Dropping the subscript *x*, the expansion of the state in the first period $[0, \tau]$ is thus $m_1 = U m_\phi$. However, a primary difference between the ODE case and the DDE case is that the monodromy operator *U* for the DDE is infinite dimensional [35]. Thus, the condition for asymptotic stability

requires that the infinite number of characteristic multipliers, or eigenvalues of U, must have a modulus of less than one. In general, however, it is impossible to find all eigenvalues of the infinite dimensional U. We use the Chebyshev collocation approximation method to approximate U by a matrix of finite dimension, whose spectral radius approximately decides the stability. Because of the compactness of operator U, all of the neglected eigenvalues are clustered about the origin assuming than N is large enough so that solutions of the DDE are well-approximated [37]. Thus the neglected eigenvalues do not influence the stability.

Now let us approximate equation (5) using the Chebyshev collocation method, in which the approximate solution is described by *its values at the collocation points in any given interval*. (Note that for a collocation expansion on an interval of length $T = \tau$, the standard interval [-1,1] for the Chebyshev polynomials is easily rescaled). As shown in Fig. 1b), let m_1 be the set of $N + 1$ values of $x(t)$ in the interval $t \in [0,T]$ and m_ϕ be the set of $N + 1$ values of the initial function $\phi(t)$ in $t \in [-T, 0]$. Recalling that the points are numbered right to left by convention, the matching condition in Fig. 1b) is seen to be that $m_{1N} = m_{\phi 0}$. (This will be modified later to account for a period of free vibration between cuts of successive teeth.) As this also applies for any two successive periods, writing equation (5) in the algebraic form representing the Chebyshev collocation expansion vectors m_{i-1} and m_i, we obtain

$$\hat{D}m_i = \hat{M}_A m_i + \hat{M}_B m_{i-1} \tag{7}$$

The $(N+1)n\times(N+1)n$ $\hat{D}$ matrix is obtained from $\mathbb{D}$ by 1) scaling to account for the shift $[-1,1]\rightarrow[0,T]$ by multiplying the resulting matrix by $2/T$, and 2) modifying the last n rows as $\begin{bmatrix}0_n & 0_n & \ldots & I_n\end{bmatrix}$ where 0_n and I_n are $n\times n$ null and identity matrices, respectively, in order to enforce the n matching conditions. The pattern of the $(N+1)n\times(N+1)n$ product operational matrix $\hat{M}_A$ corresponding to $A(t)$ is

$$\hat{M}_A=\begin{bmatrix} A(t_0) & & & & & \\ & A(t_1) & & & & \\ & & A(t_2) & & & \\ & & & \ddots & & \\ & & & & A(t_{N-1}) & \\ 0_n & 0_n & 0_n & \cdots & 0_n & 0_n \end{bmatrix} \tag{8}$$

where $A(t_i)$ is calculated at the i^{th} collocation point. Similarly, the product operational matrix corresponding to matrix $B(t)$ is

$$\hat{M}_B=\begin{bmatrix} B(t_0) & & & & & \\ & B(t_1) & & & & \\ & & B(t_2) & & & \\ & & & \ddots & & \\ & & & & B(t_{N-1}) & \\ I_n & 0_n & 0_n & \cdots & 0_n & 0_n \end{bmatrix} \tag{9}$$

Here the hat (^) above the operator refers to the fact that the matrices are modified by altering the last n rows to account for the matching conditions. (The I_n matrix in $\hat{M}_B$ will be modified later to account for a period of free vibration.)

Therefore, since U is defined as the mapping of the solution at the collocation points to successive intervals as $m_i = Um_{i-1}$, we obtain an approximation to the monodromy operator in equation (6) by using equation (7):

$$U = \left[\hat{D} - \hat{M}_A\right]^{-1} \hat{M}_B \tag{10}$$

Alternatively, the inversion of $\left[\hat{D} - \hat{M}_A\right]$ can be avoided by setting the determinant of $\left\{\hat{M}_B - \mu\left[\hat{D} - \hat{M}_A\right]\right\}$ to zero, where μ is a Floquet multiplier. It is seen that if $N + 1$ is the number of collocation points in each interval and n is the order of the original delay differential equation, then the size of the U matrix (whose eigenvalues approximate the Floquet multipliers which have largest absolute values) will be $(N+1)n \times (N+1)n$. We can achieve higher accuracy for the Floquet multipliers by increasing the value of N.

3. Milling Model

Here, we analyze a single degree-of-freedom zero-helix milling model with linear or nonlinear regenerative cutting force for multiple cutting teeth in both up- and down-milling directions. This model has also been analyzed in [19-21] while higher degree-of-freedom versions were considered in [15-17], for example. The tool is assumed to be flexible in the x-direction only. A summation of cutting forces acting on the tool produces the equation of motion

$$\ddot{x}(t) + 2\zeta\omega_n \dot{x}(t) + \omega_n^2 x(t) = \frac{F_x(t)}{m} \tag{11}$$

where m is the mass, ζ is the damping ratio, ω_n is the natural angular frequency, and F_x is the cutting force in the x-direction.

According to Fig. 2a), the x component of the cutting force on the p^{th} tooth is given by

$$F_{xp}(t) = g_p(t)(-F_{tp}(t)\cos\theta_p(t) - F_{np}(t)\sin\theta_p(t))$$

$$F_{tp}(t) = K_t b(w_p(t))^q, \quad F_{np}(t) = K_n b(w_p(t))^q \tag{12}$$

where $g_p(t)$ acts as a switching function. It is equal to one if the p^{th} tooth is actively cutting and zero if it is not cutting as defined by entry and exit angles which are specific to the cases of up- and down-milling (to be discussed). $\theta_p(t)$ is the angle of the p^{th} cutting tooth as it rotates. The tangential and normal cutting force components are the products of the tangential and normal linearized cutting coefficients K_t and K_n, respectively, the nominal depth of cut b, and the qth power of the instantaneous chip width $w_p(t) = f\sin\theta_p(t) + [x(t) - x(t-\tau)]\sin\theta_p(t)$, which depends on the feed per tooth f, the cutter angle $\theta_p(t)$, and the current and delayed tool position according to Fig. 2b). $\tau = 60/(z\Omega)$ [s] is the tooth pass period in seconds where Ω is the spindle speed given in rpm, z is the number of teeth, and q is an exponent which is equal to one for a linear cutting force or less than one for a nonlinear cutting force [13, 21].

The substitution of $w_p(t)$ into equation (12), expanding the result in a Taylor series, linearizing about the feed per tooth f, substituting the result into equation (11), and summing over the total number z of cutting teeth yields

$$\ddot{x}(t)+2\zeta\omega_n\dot{x}(t)+\omega_n^2 x(t)=-\frac{bqf^{q-1}h(t)}{m}[x(t)-x(t-\tau)] \\ -\frac{b}{m}\sum_{p=1}^{z}K_t g_p(t)[\cos\theta_p(t)+\tan\gamma\sin\theta_p(t)]\left(f\sin\theta_p(t)\right)^q \tag{13}$$

where

$$h(t)=\sum_{p=1}^{z}K_t g_p(t)[\cos\theta_p(t)+\tan\gamma\sin\theta_p(t)]\left(\sin\theta_p(t)\right)^q \tag{14}$$

is the τ –periodic specific cutting force variation, $\tan\gamma=K_n/K_t$ (see Fig. 2a)), and the angular position of the tool is $\theta_p(t)=(2\pi\Omega/60)t+2\pi(p-1)/z$. The solution is assumed of the form $x(t)=\bar{x}(t)+\xi(t)$ where $\bar{x}(t)=\bar{x}(t+\tau)$ is a τ-periodic solution that solves equation (13) and represents the unperturbed, ideal tool motion when no self-excited vibrations arise, and $\xi(t)$ is the perturbation. Substitution of the assumed solution into equation (13) and the elimination of terms involving $\bar{x}(t)$ yields

$$\ddot{\xi}(t)+2\zeta\omega_n\dot{\xi}(t)+\omega_n^2\xi(t)=-\frac{\hat{b}h(t)}{m}[\xi(t)-\xi(t-\tau)] \tag{15}$$

where $\hat{b}=bqf^{q-1}$ is the normalized depth of cut. Equation (15) is the linear variational DDE model of the milling process used for stability analysis. Stability of the $\xi(t)=0$ solution implies the stability of the chatter-free periodic motion $\bar{x}(t)$.

The relationship between the direction of tool rotation and the feed defines two types of partial immersion milling operations: up-milling and down-milling (Fig. 3). Both operations work in a similar way except for the manner in which the rotation of the cutting tool is oriented with respect to the direction of the feed. However, the dynamics and stability properties are different. Partial immersion milling operations are

characterized the radial immersion ratio '*a/D*', where *a* is the radial depth of cut and *D* the diameter of the tool, as well as the percent time ρ in the cut for a full revolution of the tool. The specific cutting force variation varies with up- and down-milling as it depends on the entry and exit angles of contact. For the up-milling partial immersion case, the first tooth starts cutting at 0º and leaves at some exit angle less than 180º. Contrary to this, for the down-milling partial immersion case, the first tooth starts cutting at some entry angle greater than 0º and exits at 180º. Additional teeth have angles shifted by integer multiples of $2\pi / z$. The specific cutting force variation *h(t)* in equation (14) depends on the screen function $g_p(t)$ which is defined as $g_p(t) = 1$ if $\theta_p^{enter} < \theta_p < \theta_p^{exit}$ while $g_p(t) = 0$ otherwise. The entry and exit angles can be found from Fig. 3 as $\theta_p^{enter} = 2\pi(p-1)/z$ and $\theta_p^{exit} = \cos^{-1}(1-2a/D) + 2\pi(p-1)/z$ for up-milling, while for down-milling the angles are $\theta_p^{enter} = \cos^{-1}(2a/D-1) + 2\pi(p-1)/z$ and $\theta_p^{exit} = \pi(1+2(p-1)/z)$. The percent time in the cut for all teeth combined is thus given as the difference between the entry and exit angles normalized to a full period times the total number of teeth as $\rho = z\cos^{-1}(1-2a/D)/(2\pi)$.

If the percent time in the cut is less than 100% $(\rho < 1)$ then there is a period of free vibration between successive cuts corresponding to the system $\dot{x} = A_0 x$ where $A_0 = A(t)$ in equation (5) when $h(t) = 0$. (Note also that $B(t) = 0$ in this case). When we apply the Chebyshev collocation method to equation (15), we rescale the Chebyshev collocation points to account for the shift $[-1,\ 1] \to [0,\ \rho\tau]$, doing the same for matrix

$\hat{D}$ in equation (7) by multiplying $\mathbb{D}$ by $2/(\rho\tau)$. The state transition matrix $\Phi(t) = e^{A_0 t}$ of free vibration can easily be found, from which the matching condition between successive intervals becomes $m_{1N} = \Phi\left((1-\rho)\tau\right) m_{\phi 0}$ as shown in Fig. 4. Therefore, the last *n* rows of $\hat{M}_B$ in equation (9) are modified to $\left[\Phi\left((1-\rho)\tau\right) \quad 0_n \quad \ldots \quad 0_n\right]$.

If $\rho = 1$ so that the teeth are cutting for the entire period (such as the case of 100% immersion for two teeth in Fig. 8), then $\Phi(0) = I$ and the last *n* rows of $\hat{M}_B$ are as in the equation (9). The case of multiple engaged teeth with $\rho > 1$ is not considered here, but will be analyzed in a future work.

4. Stability Charts and Numerical Simulations

Specific cutting forces and corresponding stability charts calculated by using the Chebyshev collocation method for up-milling and down-milling processes with 25%, 50%, 75% and 100% immersion ratios are shown in Fig. 5 for q=1 (linear cutting force) and a single cutting tooth. The parameters used to construct the stability charts are m = 2.573 kg, $\zeta = 0.0032$, $\omega_n = 920.02$ rad/s, $K_n = 1.65 \cdot 10^8$ N/m^2 and $K_t = 5.5 \cdot 10^8$ N/m^2, so that $\tan\gamma = 0.3$. The mean values of $h(t)$ for a full rotation are all positive except for the down-milling cases of 25% and 50% immersion levels. Stability charts are constructed with parameters being the spindle speed Ω (ranging from 2000 to 25000 rpm) and the depth of cut b (ranging from 0 to 5 mm). The dimension of the matrix

approximating the monodromy operator for all cases is 25×25. The (Ω,b) plane is discretized into a 300×300 grid.

The stability analysis is based on the determination of the relevant characteristic multipliers using the collocation method. We use bifurcation theory to explain the type of instability. For $\mu=1$ (fold bifurcation), it can be shown that this bifurcation cannot occur in the milling equation [19,21,22]. For secondary Hopf bifurcation (indicated by an "H" in the stability charts), μ is complex with $|\mu|=1$, while $\mu=-1$ for flip or period-doubling bifurcation (indicated by a "P" in the stability charts). All regions below the stability curves are stable (i.e. chatter free). In the up-milling case (see the first and the second rows), the relative orientation of Hopf and flip regions remains the same for all immersion ratios. For full immersion, the cutting force equals zero (i.e. the system has free vibration) for half of the period, because the surface of the tool-workpiece interaction becomes a semi-cylinder (as seen in Fig. 3). Part of that time the force is negative, which can be explained by the fact that the cutter and the workpiece move in the same direction. For a low immersion ratio, the force is always positive, while it begins to include a negative portion for *a/D* slightly below 0.75. In the case of down-milling (see the third and fourth rows), on the contrary, the force is always negative for low immersion ratios, for the reason explained above, while for *a/D* slightly below 50% it begins to include a positive portion. The mean value of the force for the entire period changes sign and becomes positive between *a/D* = 50 and 75%. The specific cutting force is the same as in the up-milling case at the 100% immersion ratio. The most distinctive feature about the stability charts is the near disappearance of the unstable Hopf lobes for the down-milling

case of 75% immersion, while the Hopf lobes for 50% and 100% immersion cases change their relative orientation with respect to the flip regions. This peculiar feature will be discussed in greater detail.

In order to investigate this phenomenon closer, and also to verify the accuracy of the stability results, we compute the response at four parameter points for three immersion levels using the MATLAB numerical integration routine DDE23 [43] on equation (13). If the response goes to a finite amplitude oscillation (the nominal chatter-free motion) as time goes to infinity, then the system is said to be stable at the given parameter points; otherwise if the response grows without bound it is unstable due to either secondary Hopf or flip bifurcation. Our first conclusion is that the results shown in Fig. 6 agree with the stability charts obtained by the collocation method. If we denote the stability of a parameter point by S, and of instability by U, then each of the four parameter points A, B, C, D are stable or unstable with respect to the following patterns: A(SSU), B(UUS), C(SUU), D(USS). It can be seen that the stability characteristics of all four parameter points reverses between 65% and 80% immersion levels. While this is not surprising for points A and D due to the fact that the Hopf lobe switches locations (as also seen in Fig. 5), it is seen that points B and C switch stability characteristics as well due to a slight shift in the boundary of the flip bifurcation lobe. While each of the three immersion levels results in two stable and two unstable cases for the specific parameter points chosen, it is clearly seen that the 73% immersion level results in the greatest stable region of the parameter plane. Clearly, there is an interval of optimal immersion ratios for a maximum area of stable regions in the parameter plane.

In Fig. 7, we plot stability diagrams for fourteen immersion ratios between 0.65 and 0.78 with $\tan\gamma = 0.3$ and q=1. As can be seen, the major Hopf lobe at the far right-hand side shrinks such that it rises above b = 2 mm by a/D = 0.67, and above b = 5 mm by a/D = 0.70. At the immersion ratio between 70% and 73% there is no major Hopf lobe to the right or left of the major flip lobe which is at 17,500 rpm (compare with Figs. 5-6), while for 74% immersion the Hopf lobe suddenly appears to the left of the flip lobe. A further increase in the immersion level subsequently causes the lobe to drop even lower, dropping below b = 2 mm near 78% immersion. Thus these immersion ratios can be considered to bound an *interval of optimal stable immersion levels* in which the major Hopf lobe completely vanishes and where the boundaries depend on the depth of cut. If the cutting depth is small, the optimal interval of immersion ratios is larger, while for larger cutting depths it is smaller. It should be noted that these optimal stable intervals also depend on the value of $\tan\gamma$ as well as the nonlinear exponent q as will be shown.

Figs. 8-10 show specific cutting forces, stability charts, numerical simulations, and optimal stable immersion levels similar to Figs. 5-7 but for the case of two teeth and a nonlinear cutting force with a nonlinear exponent of q=0.75. Many features, such as the jump of the Hopf lobe near 75% immersion for down-milling in Fig. 8, the reversal in stability for all four parameter points A(SSU), B(UUS), C(SUU), and D(USS).in Fig. 9, and the interval of optimal stable immersion levels in Fig. 10, are very similar to the previous case of a single tooth and linear cutting force. It can be concluded that these features probably exist for a wide range in the number of teeth or the cutting force nonlinearity exponent.

5. Analysis of Optimal Stable Immersion Levels

In order to help explain the stability characteristics seen above, the average value of *h(t)* over a full period of rotation of the tool for a single tooth can be found as

$$< h(t) >= \frac{1}{T}\int_0^T h(t)dt = \frac{K_t}{2\pi}\int_{\theta^{enter}}^{\theta^{exit}} (\cos\theta + \tan\gamma \sin\theta)\sin^q\theta d\theta \qquad (16)$$

Using the entry and exit angles given in section 3 and setting $q = 1$ (linear cutting force), the average specific cutting force for up-milling is

$$\frac{< h(t) >}{K_t} = \frac{1}{2\pi}\left\{\left(2\frac{a}{D}\left(1-\frac{a}{D}\right)\right) + \tan\gamma\left(\frac{1}{2}\cos^{-1}\left(1-2\frac{a}{D}\right) + \left(2\frac{a}{D}-1\right)\sqrt{\frac{a}{D}\left(1-\frac{a}{D}\right)}\right)\right\} \qquad (17)$$

while for down-milling it is

$$\frac{< h(t) >}{K_t} = \frac{1}{2\pi}\left\{\left(-2\frac{a}{D}\left(1-\frac{a}{D}\right)\right) + \tan\gamma\left(\frac{\pi}{2} - \frac{1}{2}\cos^{-1}\left(2\frac{a}{D}-1\right) + \left(2\frac{a}{D}-1\right)\sqrt{\frac{a}{D}\left(1-\frac{a}{D}\right)}\right)\right\} \qquad (18)$$

These are plotted for three different values of $\tan\gamma$ in Fig. 11. It is seen for $a/D > 0$ and $\tan\gamma > 0$, that <*h(t)*> is always positive for up-milling. For down-milling <*h(t)*> is negative for a/D less than a critical value (which depends on $\tan\gamma$) and is positive for a/D greater than this value. It should be noted that while multiple teeth would alter the average cutting force, the immersion ratio where it is zero for down-milling would be the same.

In Fig. 12b a stability chart is shown for the case of a single tooth with 100% immersion (in which up- and down-milling are identical), including the negative *b* axis, for *q*=1. The concept of negative depth of cut allows a simple way to visualize the unusual behavior of the Hopf lobe as the average cutting force changes sign as noted in

[19]. The lower portion of the figure (i.e. negative *b* axis) has the same orientation of the Hopf and flip lobes that are observed in the down-milling cases of 69% and lower immersion levels in which <*h(t)*> is negative (except that they are upside down). In addition, the slight change in the flip lobe boundaries observed in Fig. 6 can be seen clearly.

A method to analytically approximate the optimal stable immersion levels works as follows. This approximation basically reduces the milling problem to that of turning with *h(t)* replaced with its average value. First, temporarily consider the turning process for which the cutting force is constant and all of the unstable lobes are due to Hopf bifurcation in which a pair of eigenvalues are $\pm i\omega$ at the stability boundary. It is well-known that the stability boundaries can be obtained parametrically in terms of ω as [22]

$$b = \left(\frac{m\omega_n^2}{k_1}\right)\frac{(\omega^2-1)^2+4\zeta^2\omega^2}{2(\omega^2-1)} \qquad \Omega = \frac{\omega_n\omega}{j+\frac{1}{\pi}\tan^{-1}\left(\frac{\omega^2-1}{2\zeta\omega}\right)}\ , \text{j} = 1, 2,\ldots \tag{19}$$

where k_1 is the cutting stiffness. Here, the average cutting force <*h(t)*> is used in place of k_1. The minimum values of these lobes are obtained from differentiating the first of equations (19) with respect to ω, setting the result to zero, and solving for ω. The two positive solutions are given by $\omega = \sqrt{1 \pm 2\zeta}$. Substitution of these back into the first of equations (19) yields the two values of

$$b = \left(\frac{m\omega_n^2}{< h(t) >}\right) 2\zeta\left(\zeta \pm 1\right) \tag{20}$$

although only the positive value is usually given. For 100% immersion and tan $\gamma = 0.3$ equation (18) yields $\langle h(t) \rangle = 0.075 \cdot K_t$ (see Fig. 12a) such that equation (20) results in b = 0.3390, -0.3368 mm. In Fig. 12b horizontal lines are shown at these values which approximate the minima and maxima of the Hopf lobes for positive and negative b values, respectively.

For the sake of completion, we also show six curves approximating the minima and maxima of the period-doubling lobes in Fig. 12b. These were obtained by assuming a piecewise constant cutting force with three portions corresponding to the averages of the positive and negative parts of $h(t)/K_t$ (0.418492 and -0.240827, respectively) along with the interval of free vibration where $h(t) = 0$ as shown in Fig. 12a. An extension of the formula for the minima of the flip lobes in the case of interrupted turning shown in [22, equation (38c)] to the present case can be derived as

$$b = \left(\frac{m\omega_n^2}{K_t} \right) \frac{\left(1-\zeta^2\right)\left(\exp\left(\pm 120\zeta\omega_n/\Omega\right)-1\right)}{2\left(\alpha-\beta\exp\left(\pm 120\zeta\omega_n/\Omega\right)\right)} \tag{21}$$

where $(\alpha, \beta) = (0.418492, 0), (0.418492, -0.24082), (0, -0.24082)$ corresponds to the three discontinuous jumps in Fig. 12a. The use of $(\pm)$ inside the exponentials results in three curves each for positive and negative b. The period doubling lobes near 17,500 rpm for both positive and negative b correspond to the first (α, β) pair above, while those near 6000 rpm and 3500 rpm correspond to the second and third (α, β) pairs, respectively. Equation (21) reduces to equation (38c) in [22] when $\alpha = m\omega_n^2 / K_t = 1$, $\beta = 0$, a normalized speed is utilized, and the (+) is used in the exponentials.

To find the optimal stable immersion levels in down-milling for a specific cutting depth, equations (20) and (18) are solved numerically for the two immersion levels that bound the optimal stable region for a specific value of tan γ. Care must be taken so that the root corresponding to negative $\langle h(t) \rangle$ is the greater of the two. In Fig. 13a, the two sets of immersion levels corresponding to both b = 2 mm and 5 mm are shown along with the root of $\langle h(t) \rangle = 0$ for a limited range of tan γ from 0.2 to 0.4 for q=1. Thus, for a cutting depth approximately less than or equal to these cutting depths, the use of down-milling with an immersion level within the given region results in the maximum stable region in which the major Hopf lobes do not affect the stability, as was shown in Fig. 7.

In order to see the effect of a nonlinear regenerative cutting force (q<1) on the optimal stable immersion levels, equations (20) and (16) must be solved numerically. Fig. 13b shows the critical immersion levels for a nonlinear exponent q=0.75. When compared with the linear cutting force case in Fig. 13a, it is seen that for given values of tan γ, the critical immersion levels have increased by 2-3%. In addition the optimal stability window for a given cutting depth has slightly narrowed. This inverse relationship between the critical immersion level and the nonlinear exponent is also seen in Fig. 14 in which the average cutting forces for up- and down-milling in equation (16) are plotted versus the immersion ratio for three different values of the nonlinear cutting exponent q. It is clearly seen here that a decrease in q corresponds to an increase in the root for the down-milling $\langle h(t) \rangle$. It should be noted that while the effects of changing the nonlinear exponent q on stability charts are usually uniform, there is the possibility of a drastic change in stability for down-milling in the vicinity of the critical immersion

level. This is seen in Fig. 15 for a single tooth with $\tan\gamma = 0.3$, a/D = 76%, and both linear and nonlinear (with q=0.8, 0.6, 0.4) cutting forces, in which stability is increased in some regions and decreased in others.

6. Conclusions

In this paper, a new approximation technique which uses a collocation expansion at the Chebyshev collocation points was proposed for the stability analysis of linear time-periodic delay-differential equations, and of a single degree-of-freedom model for the milling process in particular. In this method, the derivatives of functions are approximated by introducing the spectral differentiation matrix. The stability analysis is based on discretization of the infinite-dimensional monodromy operator and the computation of its eigenvalues, which exponentially converge to the exact Floquet multipliers as the number of collocation points is increased. The main advantage of the method is that it can be accurately applied to the systems of delay differential equations with non-smooth coefficients such as partial immersion milling by utilizing the exact solution during the interval of free vibration in which the coefficients vanish, thus producing stability charts with high speed and accuracy in a given parameter range.

The milling model analyzed here was a single degree-of-freedom zero helix model with multiple cutting teeth for up- and down-milling with linear or nonlinear cutting force and arbitrary immersion ratio. The specific cutting force variations throughout one period of tool rotation and the corresponding stability charts were shown for various cases. The types of instability which are characteristic for this process are the

secondary Hopf and flip (period-doubling) types. It was shown that in the up-milling case, the relative orientation of Hopf and flip regions remains the same for all immersion ratios, whereas it changes in the case of down-milling at an immersion ratio near 75% which depends on the ratio of the normal to tangential cutting stiffnesses ($\tan\gamma$) and the nonlinearity exponent for the regenerative cutting force. It was shown that this phenomenon results from a change in the sign of the average specific cutting force, which is unique to down-milling, and results in an interval of optimal stable immersion levels in which the major unstable Hopf lobe completely vanishes for an interval of immersion ratios which depends on the depth of cut. The stability charts obtained by the collocation method agree with the numerical simulations produced by the MATLAB routine DDE23 and with the previous results in the literature. For verification of the collocation results and to determine the bounds of the interval of the optimal stable immersion levels, the average value of the specific cutting force for both up- and down-milling cases was computed analytically for the case of a linear cutting force, and numerically for the case of a nonlinear cutting force. Comparisons of the results using linear and nonlinear cutting forces indicate that the optimal stability window is higher (in terms of immersion level) and slightly narrower for a nonlinear cutting force, and that in special cases a change in the nonlinear exponent can drastically alter the stability chart for down-milling.

Plans for extension of the present work include an analysis of the case of multiple engaged teeth in which $\rho > 1$, and a detailed study of the parametrically-induced period-doubling islands of instability (shown in [22] for interrupted turning and in [23, 24] for milling with a nonzero helix angle), for which equation (21) in this paper introduces a

new formula for the approximate lower bounds of cutting depth for partial-immersion milling.

Acknowledgments

This paper is partially based upon work supported by the National Science Foundation under Grant No. 0114500. The helpful suggestions of the reviewers which improved this paper are highly appreciated.

References

[1] Tobias, S. A., 1965, *Machine Tool Vibration*, Wiley, NY.
[2] Tlusty, J., 1986, "Dynamics of High-Speed Milling", Journal of Engineering for Industry 108, 59-67.
[3] Tlusty, J., 1993, "High-Speed Machining", Annals of the CIRP 42, 733-738.
[4] Halley, J. E., Helvey, A. M., Smith, K. S., 1999, "The Impact of High-speed Machining on the Design and Fabrication of Aircraft Components", 17th ASME Biennial Conference on Mechanical Vibration and Noise, Sept. 12-15, 1999, Las Vegas, NV.
[5] Hahn, W., 1961, "On Difference Differential Equations with Periodic Coefficients", Journal of Mathematical Analysis and Application 8, 70-101.
[6] Minis, I., and Yanushevsky, R., 1993, "A new theoretical approach for the prediction of machine tool chatter in milling", Journal of Engineering for Industry 115, 1-8.
[7] Altintas, Y. and Budak, E., 1995, "Analytical prediction of stability lobes in milling", Annals of the CIRP 44, 357-362.
[8] Davies, M.A., Pratt, J. R., Dutterer, B., Burns, T.J., 2002, "Stability prediction for low radial immersion milling", Journal of Manufacturing Science and Engineering 124, 217-225.
[9] Zhao, M. X. and Balachandran, B., 2001, "Dynamics and stability of milling process", International Journal of Solids and Structures 38, 2233-2248.
[10] Davies, M. A., Dutterer, B., Pratt, J. R., and Schaut, A., 1998, "On the dynamics of high speed milling with long, slender endmills", Annals of the CIRP 47, 55-60.
[11] Davies, M. A., Pratt, J. R., Dutterer, B., and Burns, T. J., 2000, "Interrupted machining – a doubling in the number of stability lobes?", J. Manufacturing Science Engineering 124, 217–225.

[12] Insperger, T. and Stépán, G., 2000, "Stability of the milling process", Periodica Polytechnica 44 (1), 47-57.
[13] Insperger, T. and Stépán, G., 2004, "Vibration Frequencies in High-Speed Milling Processes or a Positive Answer to Davies, Pratt, Dutterer and Burns", Journal of Manufacturing Science and Engineering 126, 481-487.
[14] Insperger, T. and Stépán, G., 2004, "Updated semi-discretization method for periodic delay-differential equations with discrete delay", International Journal for Numerical Methods in Engineering 61, 117-141.
[15] Mann, B. P., Bayly, P. V., Davies, M. A., and Halley, J. E., 2004, "Limit cycles, bifurcations, and accuracy of the milling process", Journal of Sound and Vibration 277, 31–48.
[16] Mann, B. P., Young, K. A., Schmitz, T. L., Dilley, D. N., 2005, "Simultaneous Stability and Surface Location Error Predictions in Milling", Journal of Manufacturing Science and Engineering 127 (3), 446-453.
[17] Mann, B. P., Garg, N. K., Young, K. A., Helvey, A. M., 2005, "Milling Bifurcations from Structural Asymmetry and Nonlinear Regeneration", Nonlinear Dynamics 42 (4), 319-337.
[18] Garg, N. K., Mann, B. P., Kim, N. H., Kurdi, M. H., 2007, "Stability of a Time-Delayed System With Parametric Excitation", Journal of Dynamic Systems, Measurement, and Control 129 (2), 125-135.
[19] Insperger, T., Mann, B. P., Stépán, G., Bayly, P. V., 2003, "Stability of up-milling and down-milling, part 1: alternative analytical methods", International Journal of Machine Tools and Manufacture 43, 25-34.
[20] Mann, B. P., Insperger, T., Bayly, P. V., Stépán, G., 2003, "Stability of up-milling and down-milling, part 2: experimental verification", International Journal of Machine Tools and Manufacture 43, 35-40.
[21] Insperger, T., Stépán, G., Bayly, P. V., Mann, B. P., 2003, "Multiple chatter frequencies in milling processes", Journal of Sound and Vibration 262, 333-345.
[22] Szalai, R., Stépán, G., 2006, "Lobes and Lenses in the Stability Chart of Interrupted Turning", Journal of Computational and Nonlinear Dynamics 1 (3), 205-211.
[23] Zatarain, M., Munoa, J., Peigne, G., Insperger, T., 2006, "Analysis of the Influence of Mill Helix Angle on Chatter Stability," Annals of the CIRP 55(1), 365-368.
[24] Patel, B.R., Mann, B.P., Young, K.A., 2008, "Uncharted Islands of Chatter Instability in Milling," Int. J. Machine Tools and Manufacture 48, 124-134.
[25] Long, X.-H., Balachandran, B., Mann, B. P., 2007, "Dynamics of milling processes with variable time delays", Nonlinear Dynamics 47 (1-3), 49-63.
[26] Olgac, N., Sipahi, R., 2007, "Dynamics and Stability of Variable-Pitch Milling", Journal of Vibration and Control, 13 (7) 1031-1043.
[27] Insperger, T., Stépán, G., Hartung, F., and Turi, J., 2005, "State-Dependent Regenerative Delay in Milling Processes", proc. ASME IDETC, Sept. 24-28, 2005, Long Beach, CA.
[28] Sinha, S. C., Wu, D.-H., 1991, "An efficient computational scheme for the analysis of periodic systems", Journal of Sound and Vibration 151, 91-117.

[29] Butcher, E. A., Ma, H., Bueler, E., Averina, V., Szabó, Z., 2004, "Stability of linear time-periodic delay-differential equations via Chebyshev polynomials", International Journal of Numerical Methods in Engineering 59, 895-922.
[30] Bellen, A., 1984, "One-Step Collocation for Delayed Differential Equations", Journal of Computational Applied Mathematics 10, 275-283.
[31] Ito, K., Tran, H. T., Manitus, A., 1991, "A fully discrete spectral method for delay differential equations", SIAM Journal of Numerical Analysis 28, 1121-1140.
[32] Engelborghs, K., Luzyanina, T., in 'T Hout, K. J., Roose, D., 2000,"Collocation Methods for the Computation of Periodic Solutions of Delay Differential Equations", SIAM Journal on Scientific Computing 22, 1593-1609.
[33] Luzyanina T., Engelborghs, K., 2002, "Computing Floquet Multipliers for Functional Differential Equations", International Journal of Bifurcation and Chaos in Applied Sciences and Engineering 12, 2977-2989.
[34] Engelborghs, K., Roose, D., 2002, "On stability of LMS methods and characteristic roots for delay differential equations", SIAM Journal of Numerical Analysis 40(2), 629-650.
[35] Hale, J. K., Lunel, M. V., 1993, *Introduction to Functional Differential Equations*, New York: Springer.
[36] Trefethen, L. N., 2000, *Spectral Methods in MATLAB*, SIAM, Software-Environment-Tools Series, Philadelphia.
[37] Bueler, E., 2007, "Error Bounds for Approximate Eigenvalues of Periodic-Coefficient Linear Delay Differential Equations", SIAM Journal of Numerical Analysis 45 (6), 2510-2536.
[38] Gilsinn, D. E., Potra, F. A., 2006, "Integral Operators and Delay Differential Equations", Journal of Integral Equations and Applications 18 (3), 297-336.
[39] Butcher, Eric A., Nindujarla, P., and Bueler, E., 2005, "Stability of Up- and Down-Milling Using Chebyshev Collocation Method," proceedings of 5th International Conference on Multibody Systems, Nonlinear Dynamics, and Control, ASME DETC'05, Long Beach, CA, Sept. 24-28, 2005.
[40] Deshmukh, V., Butcher, E. A., and Bueler, E., 2008, "Dimensional Reduction of Nonlinear Delay-Differential Equations with Periodic Coefficients using Chebyshev Polynomials," Nonlinear Dynamics 52, 137-149.
[41] Deshmukh, V., 2008, "Spectral Collocation-Based Optimization in Parameter Estimation for Nonlinear Time-Varying Dynamical Systems," Journal of Computational and Nonlinear Dynamics 3, 011010-1-7.
[42] Bueler, E., 2005, *Guide to* DDEC: *Stability of linear, periodic DDEs using the DDEC suite of MATLAB codes,* http://www.dms.uaf.edu/~bueler/DDEcharts.htm.
[43] Shampine, L. F., Thompson, S., 2001, "Solving Delay Differential Equations with DDE23", Appl. Numer. Math. 37(4), 441-458.

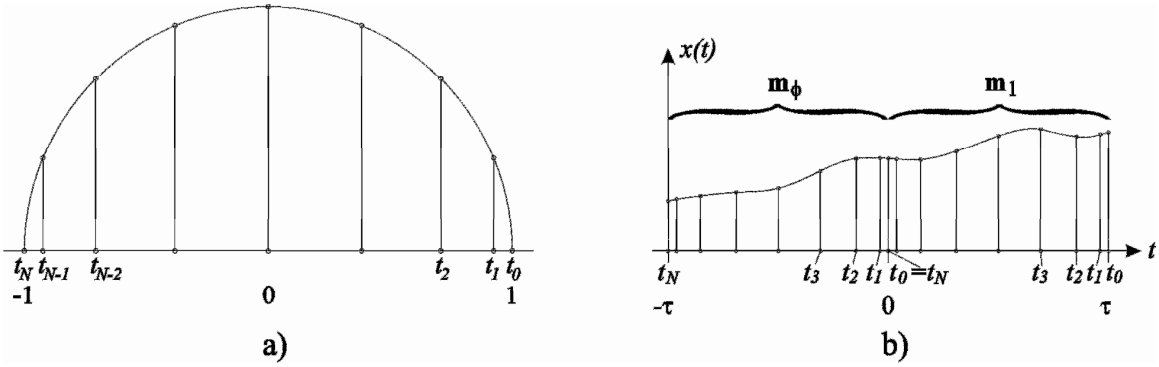

Figure 1. Diagrams of a) Chebyshev collocation points as defined by projections from the unit circle and b) collocation vectors on successive intervals.

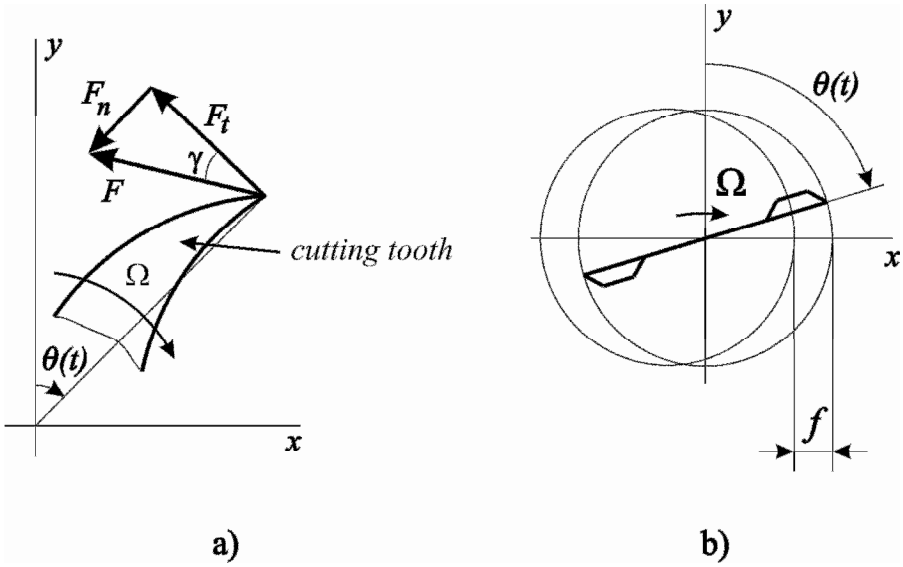

Figure 2. Geometry of a) cutting forces and b) feed per tooth.

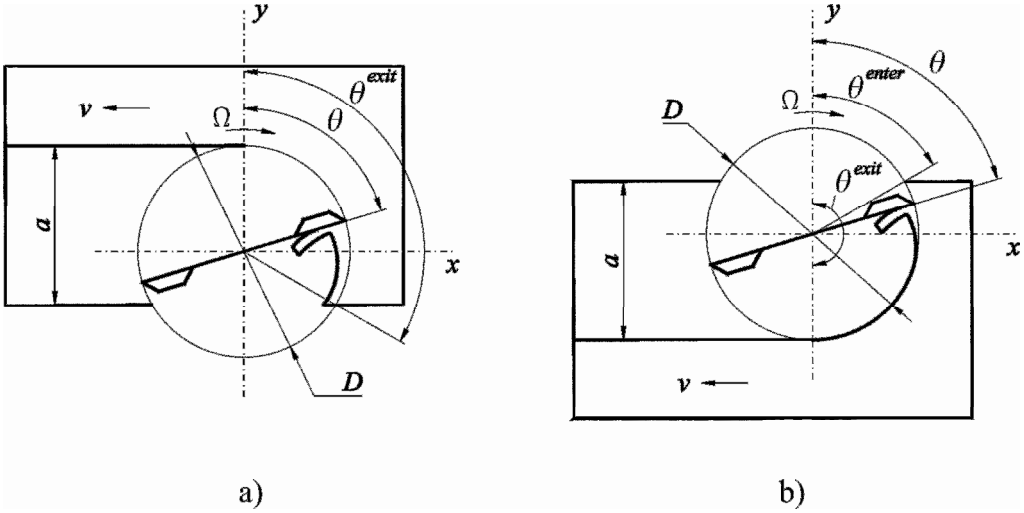

Figure 3. Illustrations of (a) up-milling and (b) down-milling.

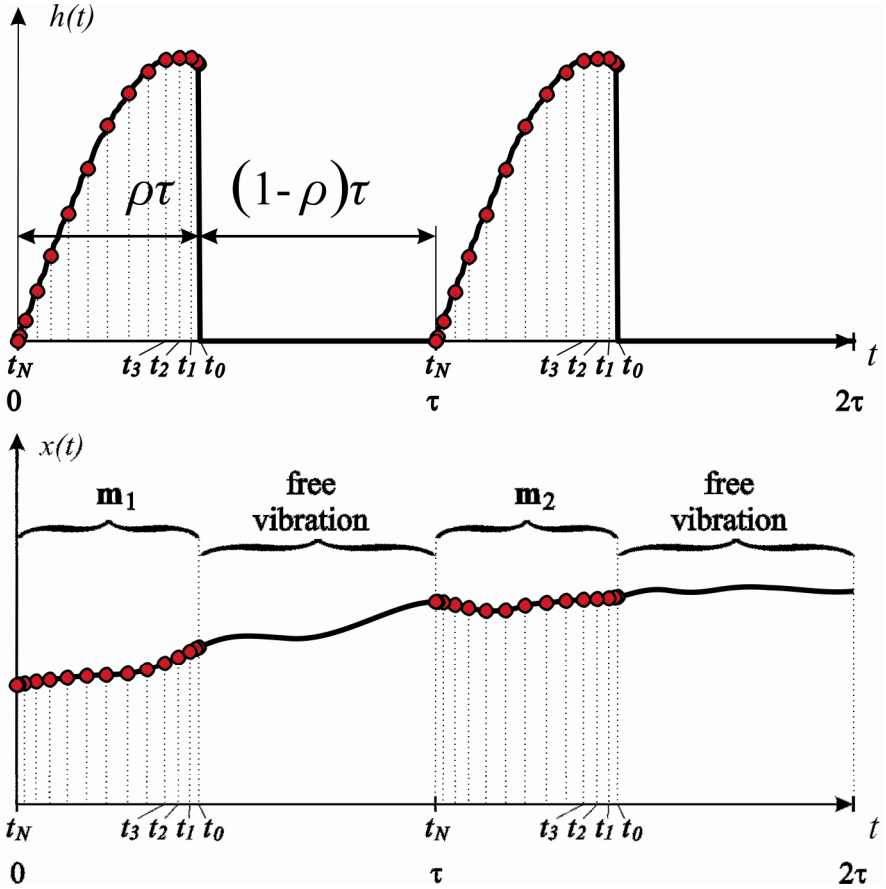

Figure 4. Chebyshev collocation expansion of the specific cutting force *h(t)* and collocation vectors on successive intervals of the solution *x(t)* for the case of a period of free vibration.

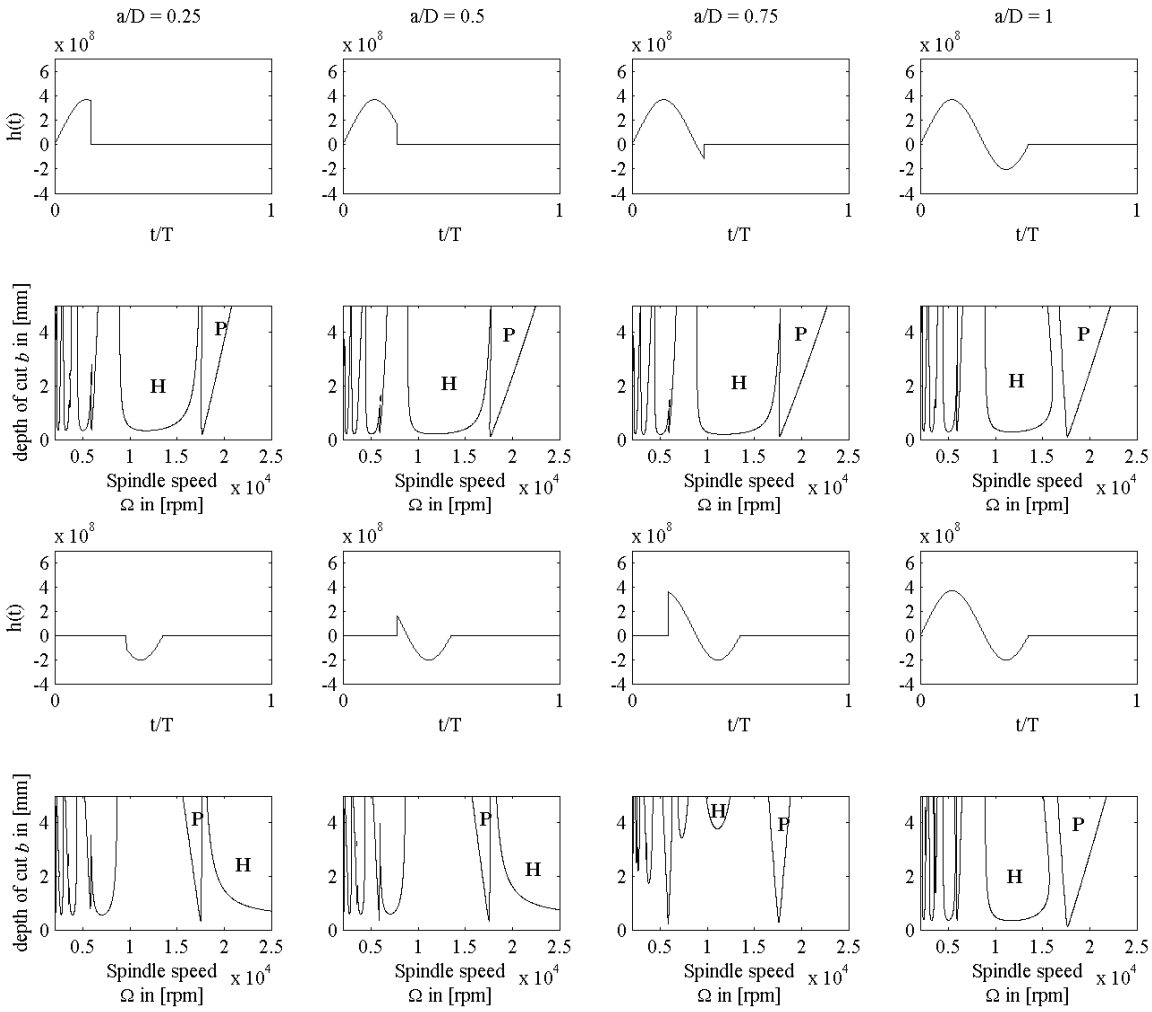
a/D = 0.25
a/D = 0.5
a/D = 0.75
a/D = 1
h(t)
t/T
depth of cut b in [mm]
Spindle speed Ω in [rpm]
x 10^8
x 10^4
H
P

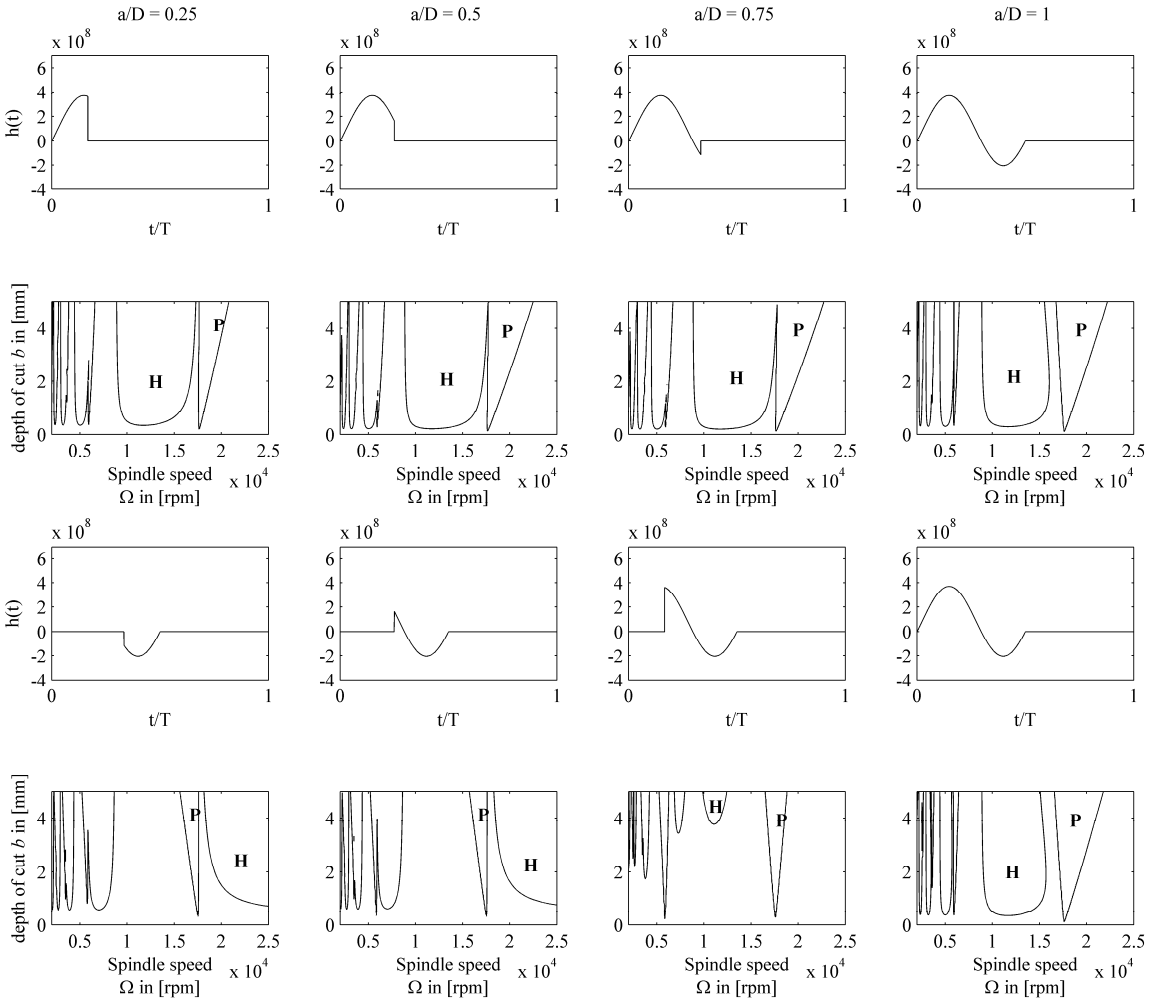

Figure 5. Specific cutting forces and stability charts for up-milling (rows 1 and 2) and down-milling (rows 3 and 4) for one cutting tooth and immersion ratios of a/D = 0.25, 0.5, 0.75, and 1; q = 1 (linear cutting force)

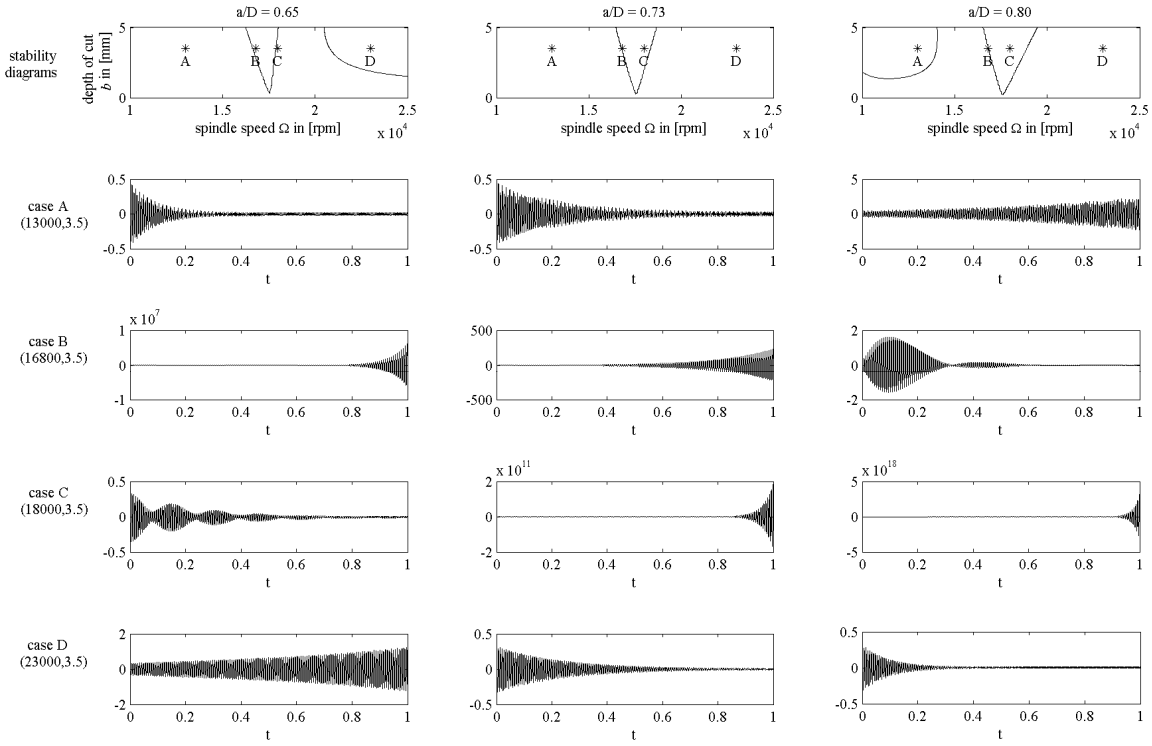

Figure 6. DDE23 simulations of equation (13) for the four parameter points A(13000,3.5), B(16800,3.5), C(18000,3.5), D(23000,3.5) for down-milling, one tooth, and $q = 1$ (linear cutting force).

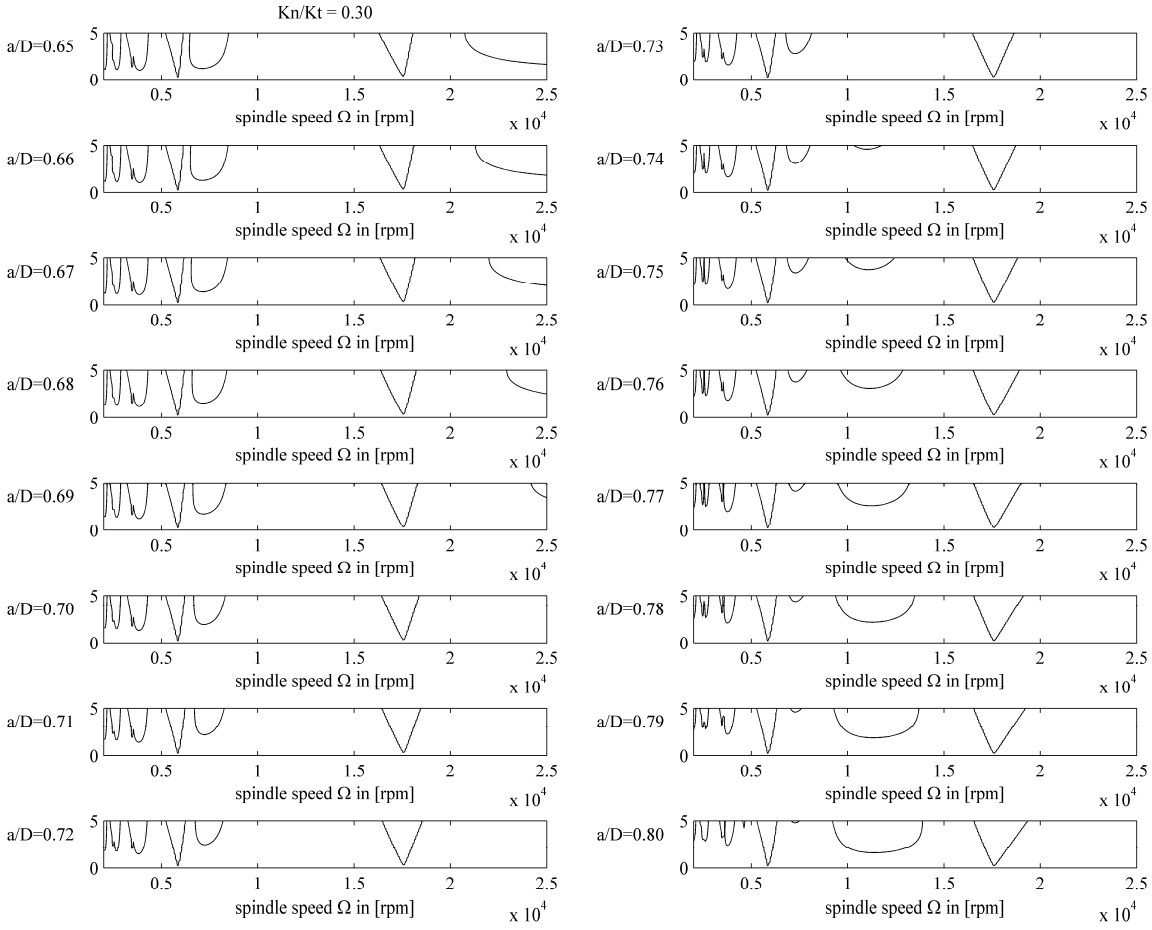

Figure 7. Optimal stable immersion levels for down-milling, one cutting tooth, $\tan\gamma = 0.3$, for $q = 1$ (linear cutting force).

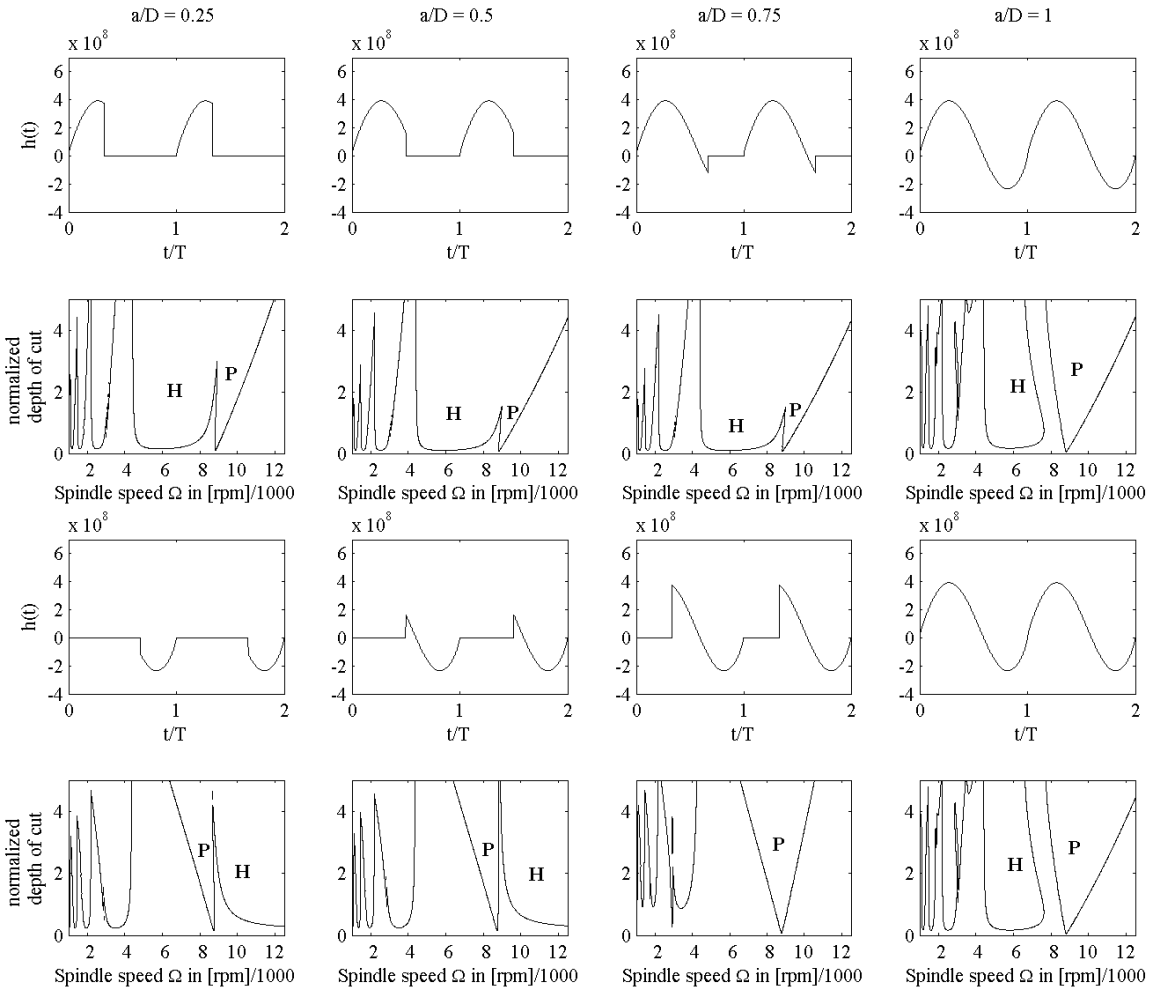

Figure 8. Specific cutting forces and stability charts for up-milling (rows 1 and 2) and down-milling (rows 3 and 4) for two cutting teeth and immersion ratios of *a/D*=0.25, 0.5, 0.75, and 1; $q = 0.75$ (nonlinear cutting force).

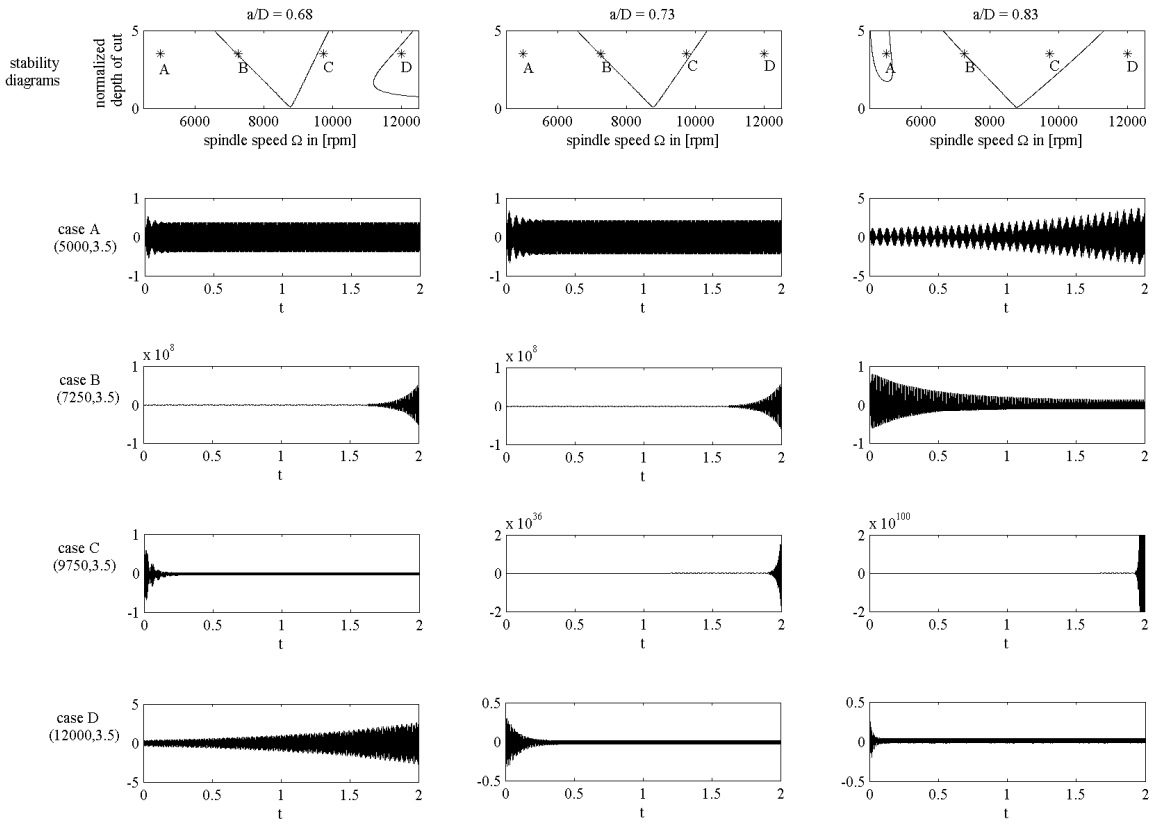

Figure 9. DDE23 simulations of equation (13) for the four parameter points A(5000,3.5), B(7250,3.5), C(9750,3.5), D(12000,3.5) for down-milling, two cutting teeth, and $q = 0.75$ (nonlinear cutting force).

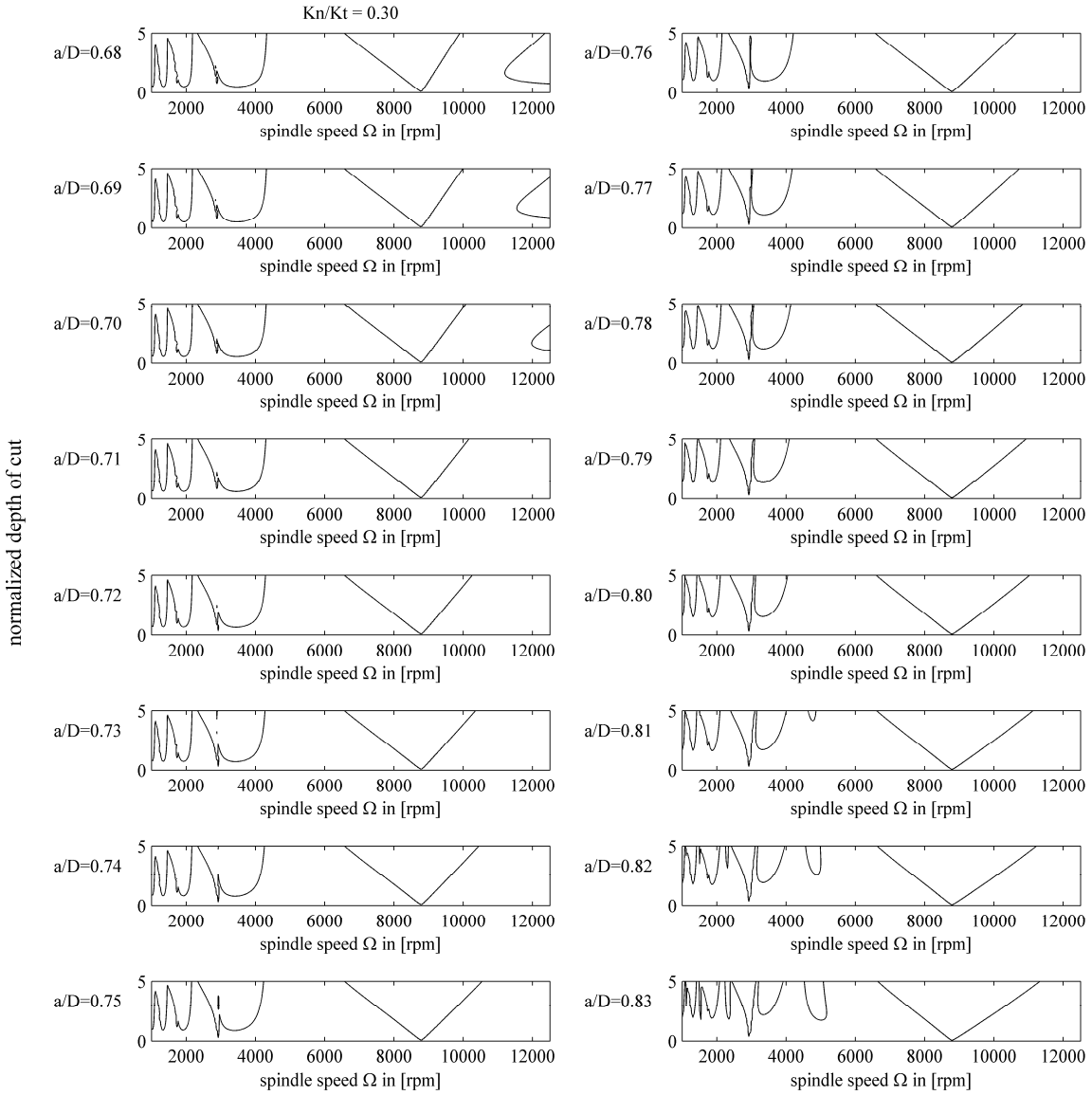

Figure 10. Optimal stable immersion levels for down-milling, $\tan\gamma = 0.3$, two cutting teeth, and $q = 0.75$ (nonlinear cutting force).

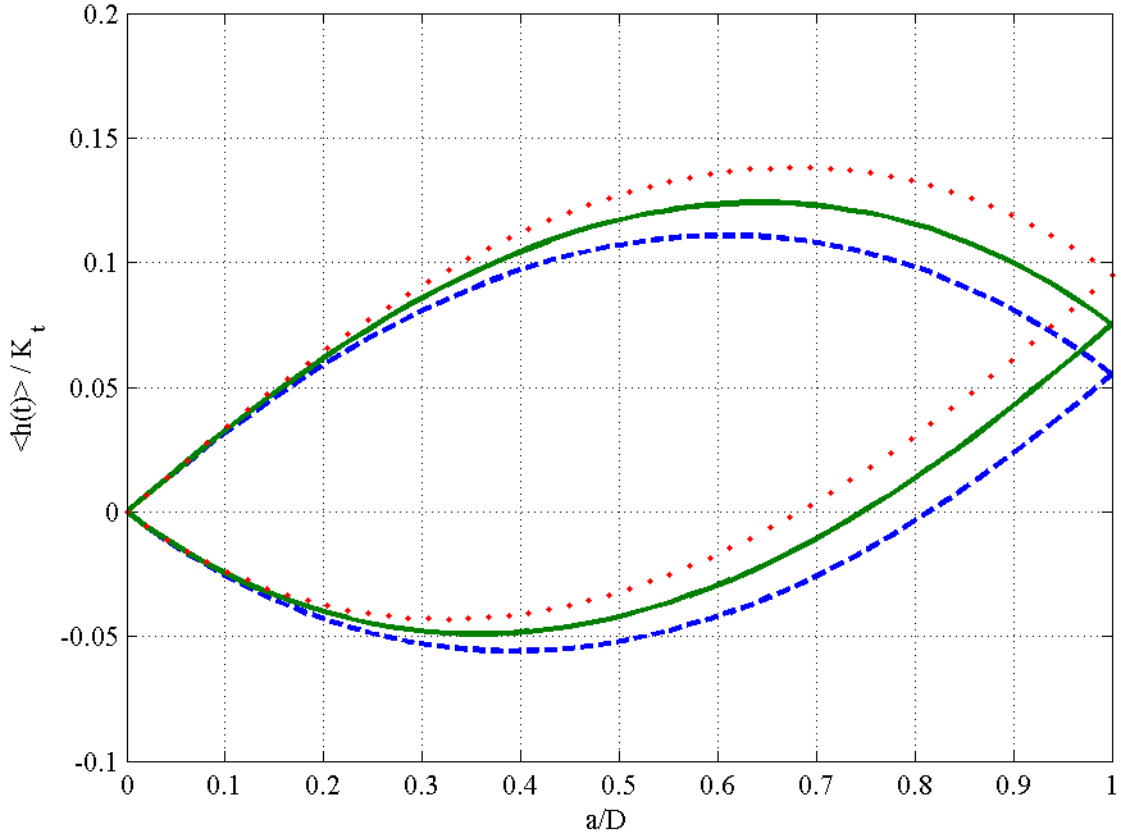

Figure 11. Average cutting forces for up- (top curve) and down- (bottom curve) milling for a single tooth with $\tan\gamma = 0.22$ (dashed), 0.3 (solid), and 0.38 (dotted).

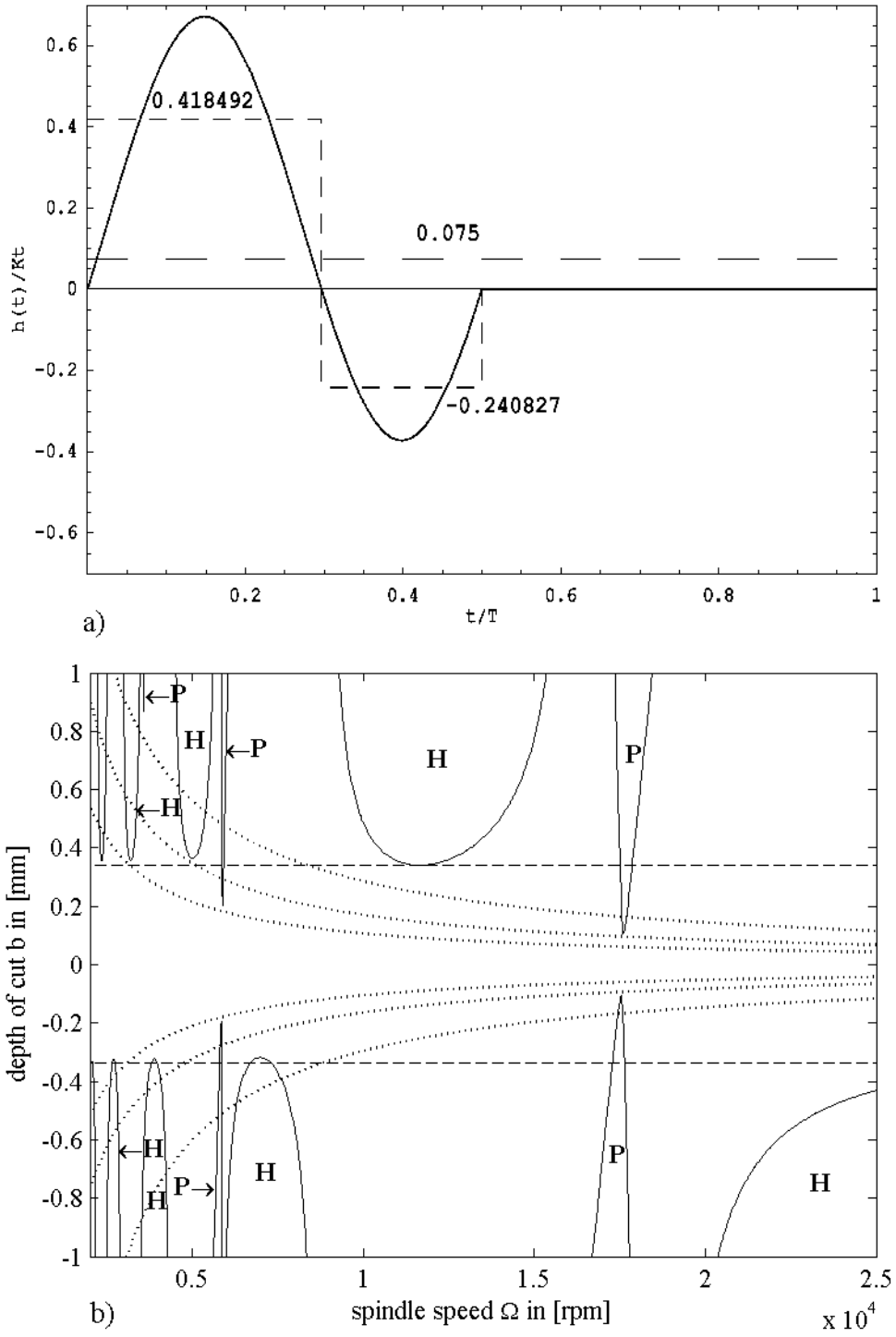

Figure 12. a) Specific cutting force profile for *a/D* = 1.00 with two ways of averaging: throughout the entire period (long-dashed line) and inside the positive and negative parts

separately (short-dashed line). b) The corresponding stability chart illustrating a negative depth of cut. The dashed lines are estimates of the minima/maxima of the Hopf lobes obtained from averaging over the period while the dotted curves are corresponding estimates for the period-doubling lobes obtained using the second averaging method.

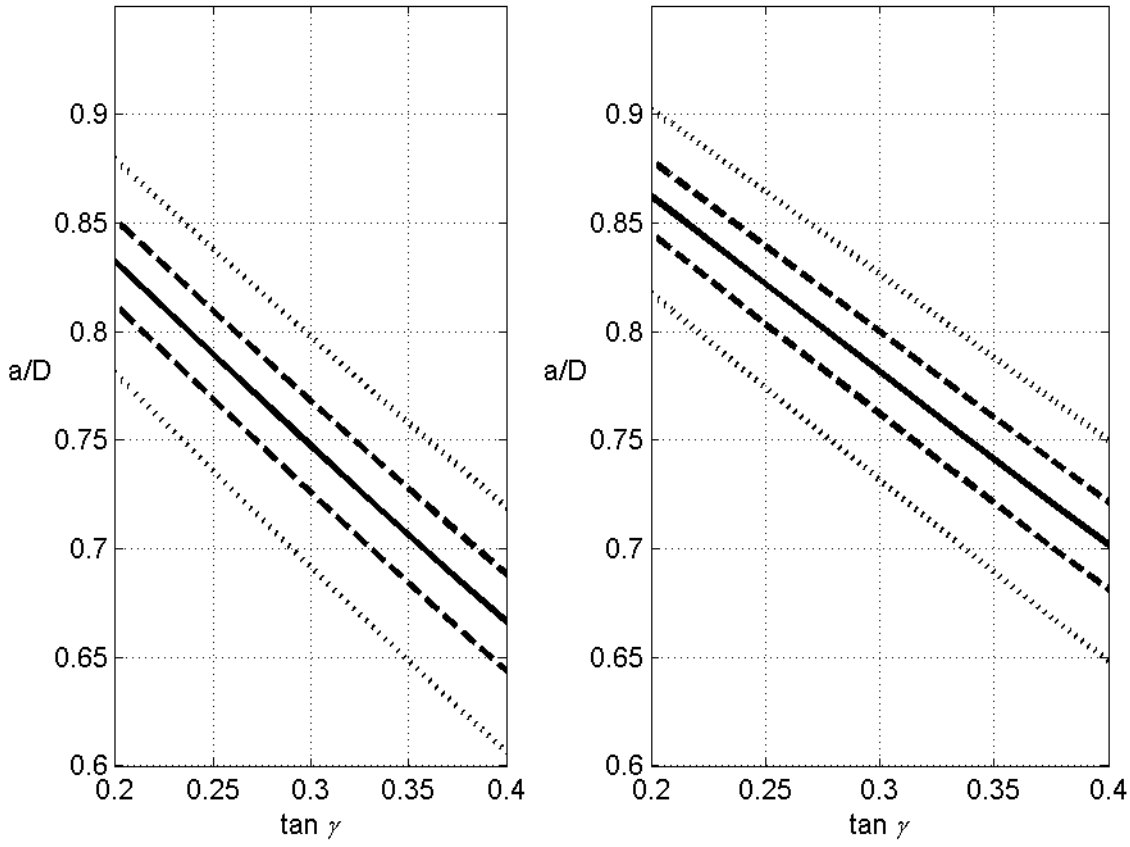

Figure 13. Immersion ratio where $\langle h(t) \rangle = 0$ (solid) and $\langle h(t) \rangle = 2m\omega_n^2 \zeta (\zeta \pm 1)/b$ for down-milling versus $\tan\gamma$ (dashed for $b = 5$ mm; dotted for $b = 2$ mm) for a single tooth with a) $q = 1$ (linear cutting force); b) $q = 0.75$ (nonlinear cutting force).

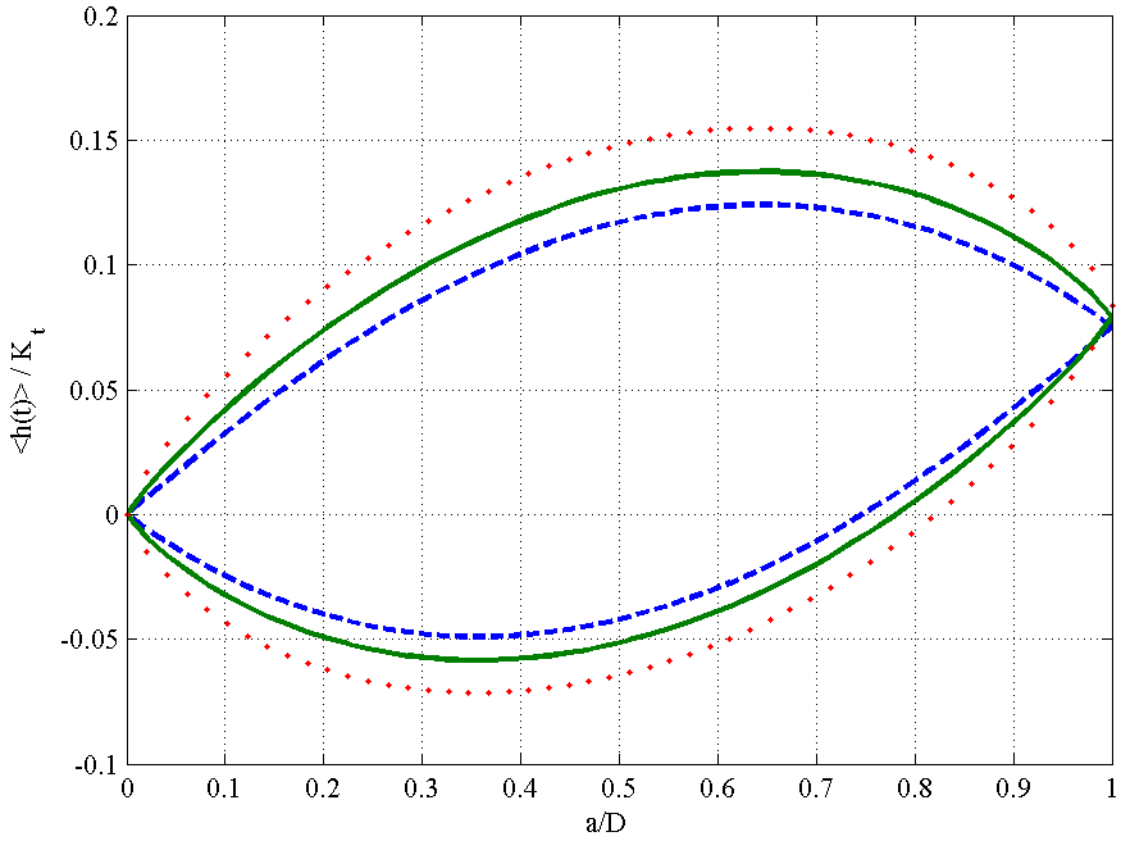

Figure 14. Average cutting force for up- (top curve) and down- (bottom curve) milling for $\tan\gamma = 0.3$, a single tooth, the linear case q = 1 (dashed), and the nonlinear cases q = 0.75 (solid) and q = 0.5 (dotted).

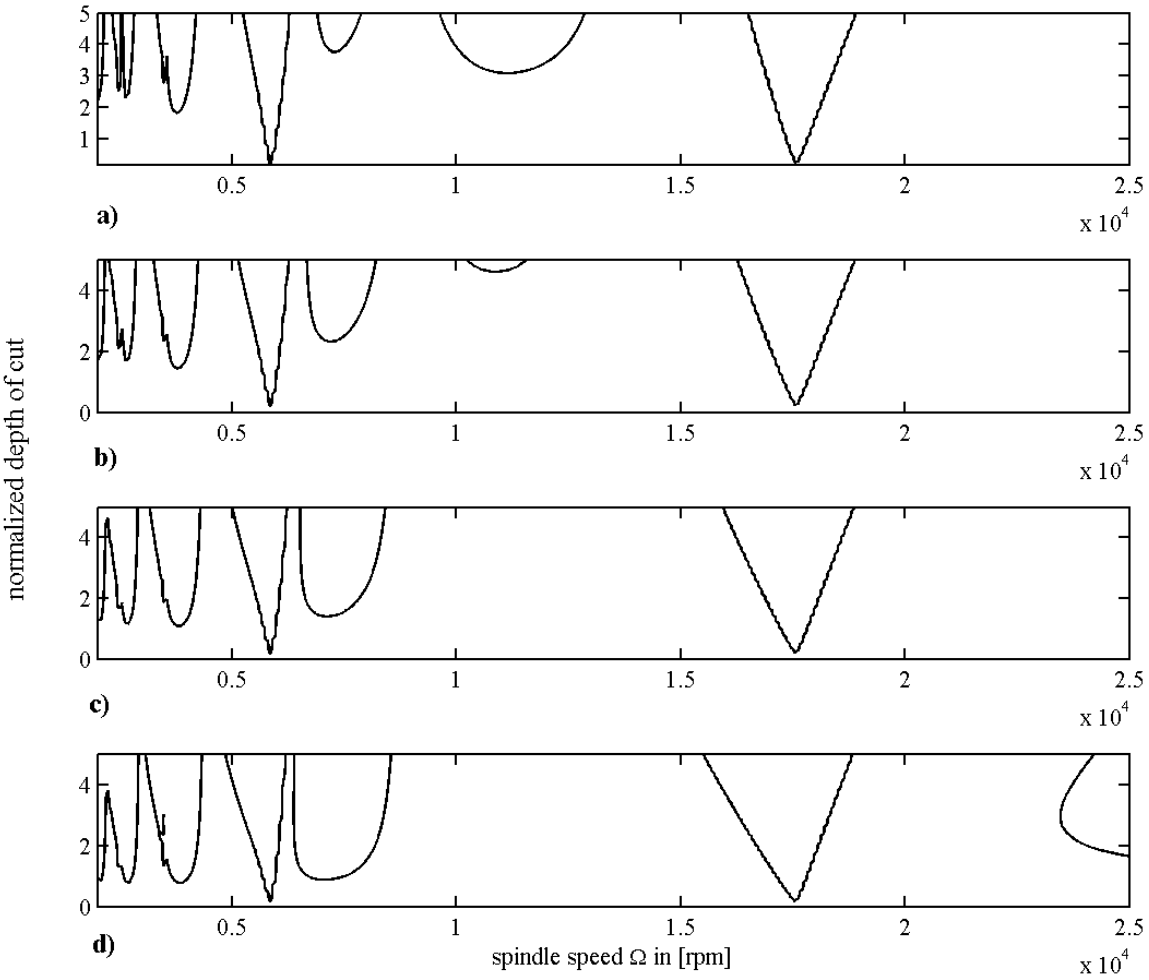

Figure 15. Stability charts for down-milling for $\tan\gamma = 0.3$, a single tooth, 76% immersion ratio, and a) $q = 1$, b) $q = 0.8$, c) $q = 0.6$, d) $q = 0.4$.